Materials Proceedings

MDPI

Proceeding Paper

Synthesis, Characterization, and Functionalization of Chitosan and Gelatin Type B Nanoparticles to Develop Novel Highly Biocompatible Cell-Penetrating Agents †

Cristina González [1], Luis H. Reyes [2], Carolina Muñoz-Camargo [1] and Juan C. Cruz [1,*]

[1] Department of Biomedical Engineering, Universidad de los Andes, Cra. 1E No. 19a–40, Bogotá, DC 111711, Colombia; c.gonzalez19@uniandes.edu.co (C.G.); c.munoz2016@uniandes.edu.co (C.M.-C.)
[2] Department of Chemical and Food Engineering, Universidad de los Andes, Cra. 1E No. 19a–40, Bogotá, DC 111711, Colombia; lh.reyes@uniandes.edu.co
* Correspondence: jc.cruz@uniandes.edu.co
† Presented at the 2nd International Online-Conference on Nanomaterials, 15–30 November 2020; Available online: https://iocn2020.sciforum.net/.

Abstract: Nowadays, nanoparticles (NPs) are used to make safe and more effective biomedical technologies for applications in highly targeted therapeutics and drug-delivery vehicles. This helps avoid low cellular penetration and accumulation of the drug in intracellular endosomal compartments that are not of interest to a particular therapy. A way to enhance therapeutic efficiency is through nanoparticle loading systems. This study aims to develop low molecular weight (LMW) and high molecular weight (HMW) chitosan and type B gelatin NPs. To enhance cell penetration, the NPs were interfaced with the translocating peptide Buforin II. The obtained nanobioconjugates were characterized by Fourier transform infrared spectroscopy (FTIR), scanning electron microscope (SEM), confocal microscopy, and transmission electron microscopy (TEM). Their size and surface zeta potential were estimated via DLS (Zetasizer Nano). Furthermore, to visualize their endosomal escape, the NPs were marked with the fluorophore Rhodamine B and imaged with the aid of confocal microscopy. The FTIR results showed bands corresponding to the polymers and Buforin II after conjugation. The average NPs diameters were about 250 nm. The zeta potential of the chitosan NPs approached neutrality, which may be problematic due to low colloidal stability. The gelatin zeta potential of −7 mV was closer to the value required for colloidal stability, i.e., ±10 mV. SEM microscopy of LMW and HMW chitosan NPs showed a round-shape and oval morphology, respectively, while the gelatin NPs had a filamentous morphology. SEM also shows agglomerates of the NPs. TEM microscopy results confirmed the LMW chitosan NPs morphology and showed that their nominal size was 5–10 nm.

Keywords: chitosan; gelatin; nanoparticles; Buforin II; Rhodamine B; endosomal escape

Citation: González, C.; Reyes, L.H.; Muñoz-Camargo, C.; Cruz, J.C. Synthesis, Characterization and Functionalization of Chitosan and Gelatin Type B Nanoparticles to Develop Novel Highly Biocompatible Cell-Penetrating Agents. *Mater. Proc.* **2021**, *4*, 30. https://doi.org/10.3390/IOCN2020-07816

Academic Editors: Ana María Díez-Pascual, Antonio Di Bartolomeo and Guanying Chen

Published: 10 November 2020

1. Introduction

Nanotechnology has emerged as a powerful route to develop safer and more effective treatments for monitoring, diagnosing, and preventing diseases [1]. For instance, nanostructured materials can be applied as drug-delivery agents (i.e., nanocarriers) or increase the contrast in medical imaging techniques. Keeping in mind the complexity of the human body, an important challenge to overcome is that drugs reach high bioavailability at the site of action [2]. Due to the cell barriers and the body's defense mechanisms, only a small number of administered drugs reach the targeted cells in a medical treatment [3]. Some strategies to improve cell-penetrating efficiency include the use of cell-penetrating peptides as well as viral or non-viral vectors, such as nanomaterials [4,5].

A large arsenal of nanomaterials from different families is currently available, including metallic-oxide, carbon-based, or polymeric, which exhibit different morphologies, topologies, and surface chemistries [3,5]. For instance, polymeric nanomaterials have shown high effectiveness in protecting and maintaining the stability of peptides, proteins, or DNA during potential degradation processes. The characteristics such as size, surface charge, and morphology can be controlled to define the uptake and internalization pathways and the nanocarriers' final fate [3,4].

Among internalization mechanisms, the most relevant for nanomaterials include clathrin- and caveolae-dependent or independent pathways, macropinocytosis, and membrane fusion. However, even if the nanocarrier penetrates the cell, it might end up trapped in the endocytic pathway, a process in which the cell membrane invaginates extracellular material by forming endosomes. The problem is that when endosomes mature, they can fuse with lysosomes, which contain enzymes that degrade the contents of the endosomes, i.e., the therapeutic cargoes transported by the nanocarrier [6]. To achieve a greater drug distribution, it is of great importance that the nanocarrier can escape the endocytic pathway. Some endosomal escape methods include membrane fusion, membrane disruption, proton sponge effect, and pore formation. This escape can also be engineered with the aid of drugs and peptides that increase cell permeability or via nanoparticles (NPs) capable of inducing membrane rupture.

Moreover, it is possible to employ polymers with pendant amine groups, which can buffer the endosomal compartment and favor escape via proton sponge effect [7]. An appealing approach is to combine both translocating agents and nanomaterials. In this regard, we have developed novel nanobioconjugates by interfacing magnetite with cell-penetrating proteins and peptides [8–13]. When developing nanocarriers for endosomal escape, a significant obstacle is the limited availability of analytical methods to quantitatively measure the escape efficiency while detecting the endosomal pathways involved. One strategy involves labeling the nanocarriers with fluorescent molecules to estimate their colocalization with endosomes via confocal imaging [7]. Moreover, an indirect indicator of escape is the transfection assay. Electrotransfection is a non-viral method applied in gene delivery. A hypothesis proposes that multiple endocytic pathways can take part in the uptake and cellular transport of electrotransfected plasmid DNA [14]. As DNA transport to the nucleus can be challenging, cytoplasmic release can be studied with RNA interference (RNAi) through the delivery of short interfering RNAs (siRNAs) that silence reporter genes [7,15]. In addition, leakage of dye from dye-loaded liposomes and the lysis of red blood cells are methods that can provide an understanding of the ability of NPs to destabilize the endosomal membrane [16].

Here, we synthesized polymeric NPs with type B gelatin and chitosan of low and high molecular weight, which were then conjugated with Buforin II—a translocating peptide with endosomal escape capacity—and the fluorophore Rhodamine B to study their endosomal escape. Type B gelatin was used due to its low price, biodegradability, and biocompatibility. Simultaneously, chitosan has antibacterial and mucoadhesive properties; plus, the different molecular weights can potentially lead to favor different routes of intracellular trafficking and endosomal escape [7,17]. The NPs' synthesis and functionalization were corroborated via Fourier-transform infrared spectroscopy (FTIR). Their morphology was studied via SEM and TEM microscopy imaging, and their size and surface charge—which can be related to their colloidal stability—were evaluated with the DLS instrument Zetasizer Nano.

2. Materials and Methods

2.1. Materials

Hydrochloric acid (HCl), glutaraldehyde, acetone, phosphate-buffered saline 1X (PBS), sodium hydroxide (NaOH), vacuum filtration unit with 0.45 μm filters, Type I, and Type II water were used. Type B gelatin and sodium tripolyphosphate (TPP) were pur-

chased from Químicos Campota (Bogotá, Colombia). Low and high molecular weight chitosan were obtained from Sigma-Aldrich, and Buforin II—with a purity of 97%—was purchased from GL Biochem. All the chemicals were used as received without any further purification.

2.2. Synthesis of Type II Gelatin and Chitosan Nanoparticles

The desolvation method was used to synthesize the gelatin NPs. Here, 10 mL of the desolvating agent acetone was added dropwise to an aqueous solution of 200 mg of gelatin in 10 mL of water. A two-phase solution was obtained where the supernatant was discarded, and the precipitate was mixed with 10 mL of an HCl aqueous solution at pH 3 and 10,000 RPM. After that, 30 mL of acetone and 100 μL of a 25% (*v*/*v*) glutaraldehyde solution were added and left mixing for 30 min to crosslink the NPs. The formed NPs were washed by centrifugation at 10,000 RPM and stored in PBS at 4 °C until further use [18].

The ionic gelation method was used to synthesize chitosan NPs. Briefly, chitosan was dissolved in a 1.25% (*v*/*v*) aqueous acetic acid solution at a concentration of 1.25 mg/mL. The mixture was left stirring for 24 h, and the pH was adjusted to 4.7 with a 1 N NaOH solution. Then, the solution was vacuum filtered with a 0.45 μm PTFE filter, and a 0.56 mg/mL TPP aqueous solution was slowly added and left mixing for 30 min. After that, the NPs were washed by centrifugation at 3200 RPM and stored in type I water at 4 °C until further use [19].

2.3. Functionalization of Nanoparticles with Buforin II

The NPs were functionalized with Buforin II (BUF-II) by adding 50 μL of glutaraldehyde in a 30 mL aqueous solution containing 100 mg of NPs. The mixture was stirred, and after 1 h, 1 mg of Buforin II was added and left under agitation for 48 h. Next, the obtained NPs–BUF-II–nanobioconjugates were washed by centrifugation five times and stored in type I water at 4 °C until further use.

2.4. Labeling of NPs-BUF-II-Nanobioconjugates with Rhodamine B

The NPs–BUF-II–nanobioconjugates were labeled with the fluorophore Rhodamine B by first dissolving 10 mg of NHS and 20 mg of EDC in 10 mL of type II water. Then, 1 mL of dimethylformamide and 20 mg of rhodamine were added and mixed at 40 °C for 15 min. This procedure was completed in the darkness to prevent the photodegradation of the fluorophore [20]. Finally, the nanobioconjugates were washed by centrifugation five times and sonicated in cold water before use.

2.5. Characterization

The Fourier Transform Infrared Spectroscopy (FTIR) from Bruker Alpha II (Bruker, Karlsruhe, Germany) was used to identify the functional groups in the NPs' samples and corroborate their functionalization. The presence of all NPs' functional groups was verified by collecting the absorbance spectrum from 600 to 4000 cm^{-1} and a spectral resolution of 2 cm^{-1}. Then, the spectra were softened. The DLS instrument Zetasizer Nano was used to measure their size distribution and surface charge in solution. The morphology of lyophilized and gold-spin-coated NPs was observed with the scanning electron microscope (SEM) JEOL JSM-6490LV. The transmission electron microscope (TEM) Tecnai F30 from FEI Company (Fremont, CA, USA) was used to observe the NPs' structure and morphology, with a resolution of 134 eV and reference energy of 5.9 keV. The confocal microscope Olympus FV1000 was used with a PlanApo 60X/1.42 N oil-immersion objective to see the dispersion of the rhodamine B-labeled NPs and study their preliminary cellular internalization in THP-1 monocytes (derived from the peripheral blood of a childhood case of acute monocytic leukemia). The samples were imaged with a 559 nm laser that could excite the fluorophore, and then, they were visualized with ImageJ [21].

3. Results and Discussion

3.1. Size Distribution and Surface Charge (Z Potential)

For three replicas (n = 3), gelatin NPs approached an average diameter of 297 ± 79 nm, while HMW chitosan and LMW chitosan NPs approached average diameters of 255 ± 52 nm and 182 ± 62 nm, respectively. The surface charge of gelatin NPs in PBS was −7.07 ± 0.17 mV, while for HMW chitosan NPs, it was −0.16 ± 0.14 mV, and for LMW chitosan NPs, it was −0.40 ± 0.16 mV. According to several studies, NPs' size is usually between 100 and 500 nm, and these sizes tend to have facilitated cellular penetration routes such as phagocytosis and clathrin- or caveolin-mediated endocytosis [22,23]. Nanomaterials with absolute surface charge below 10 mV exhibit low colloidal stability, causing aggregation and faster sedimentation [22,24]. Gelatin NPs appear to have higher colloidal stability, probably because the accumulationof type B gelatin NPs is reduced at pH values far from its isoelectric point [25]. Moreover, the number of positively charged chitosan groups might have decreased after crosslinking with TPP [26].

3.2. Fourier Transform Infrared Spectroscopy (FTIR)

The absorbance spectra of the different types of NPs had similar absorbance bands compared to the spectra of pure polymers. In this regard, we found the amide (C=O) stretching vibration at 1643 cm^{-1} and the amide (N-H) bending vibration at 1616 cm^{-1} for type B gelatin (Figure 1a), and the C=O stretching vibration at 1661 cm^{-1} and N-H bending vibration at 1562 cm^{-1} for chitosan (Figure 1b). HMW and LMW chitosan NPs showed absorbance peaks at 1579 and 1570 cm^{-1} that corresponded to the bending vibrations of N-H groups. Additionally, we identified bands at 1665 cm^{-1} and 1650 cm^{-1}, which corresponded to the stretching vibrations of C=O groups (Figure 1b). Moreover, type B gelatin NPs showed absorbance peaks at 1595 and 1676 cm^{-1} that corresponded to the bending vibrations of N-H groups and the stretching vibrations of C=O groups, respectively (Figure 1a). For BUF-II, we identified the amine (C-N) stretching vibration at 1115 cm^{-1}, the N-H bending vibration at 1567 cm^{-1}, and the C=O stretching vibration at 1678 cm^{-1} (Figure 1c–e). For the NPs-BUF-II-nanobioconjugates, we identified the C-N stretching vibration at 1123 cm^{-1} and the C=O stretching vibration at 1653 cm^{-1} for type B gelatin NPs (Figure 1c); the C-N stretching vibration at 1127 cm^{-1} and the C=O stretching vibration at 1653 cm^{-1} for HMW chitosan NPs (Figure 1d); and the C-N stretching vibration at 1127 cm^{-1} and the C=O stretching vibration at 1651 cm^{-1} for LMW chitosan NPs (Figure 1e), which confirmed effective conjugation of BUF-II.

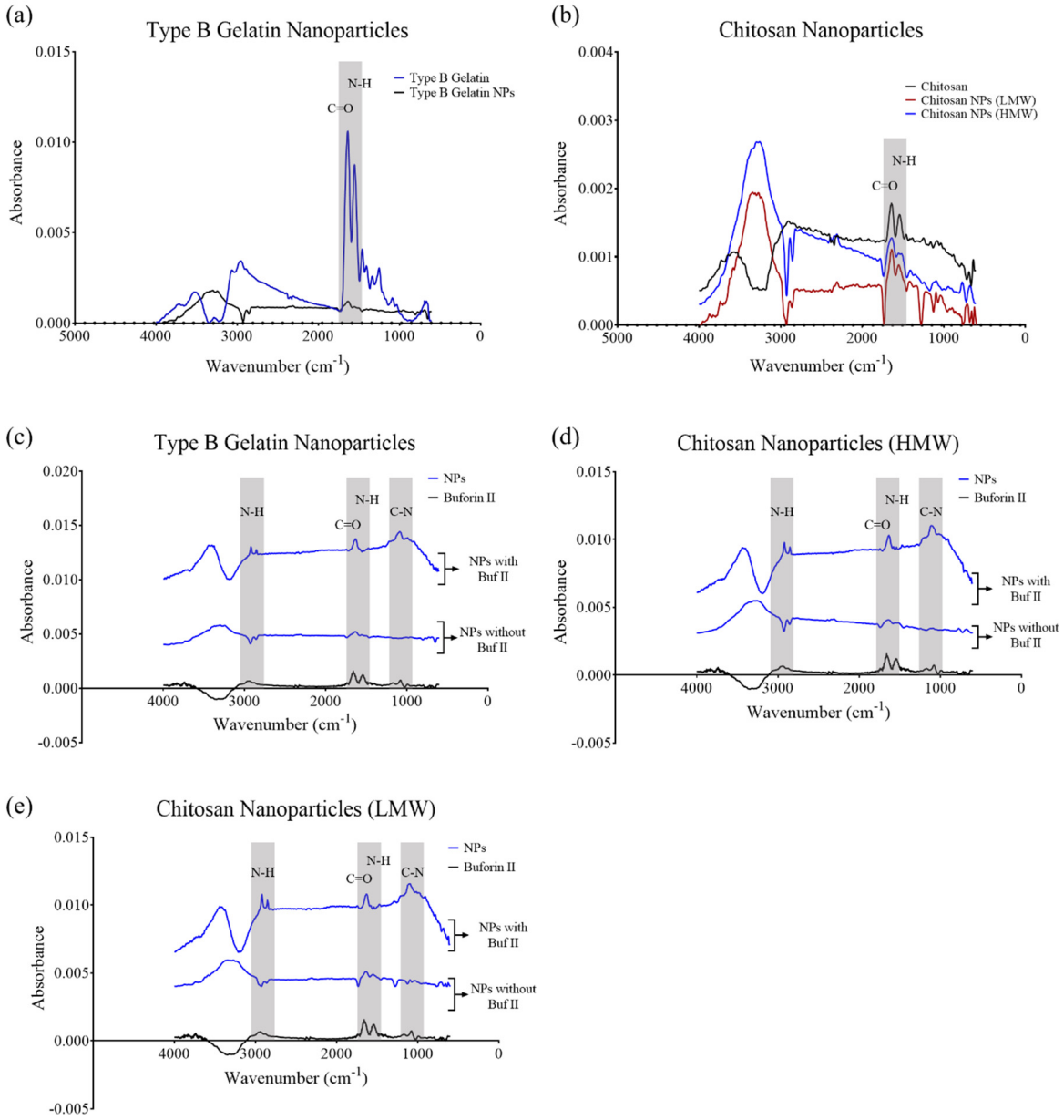

Figure 1. (**a**) Spectrum of type B gelatin NPs (blue) and pure type B gelatin (black). The absorbance band analyzed contains the C=O stretching vibrations in the range of 1640–1690 cm^{-1} and the N-H bending vibrations in the range of 1550–1640 cm^{-1}. (**b**) Spectra of LMW chitosan NPs (red), HMW chitosan NPs (blue), and pure chitosan (black). The absorbance band analyzed contains the C=O stretching vibrations in the range of 1640–1690 cm^{-1} and the N-H bending vibrations in the range of 1550–1640 cm^{-1}. (**c**) Spectrum of type B gelatin NPs before and after functionalization with Buforin II (blue) and pure Buforin II (black). Here, the absorbance bands analyzed contain the C=O stretching vibrations in the range of 1640–1690 cm^{-1}, the N-H bending vibrations in the range of 1550–1640 cm^{-1}, the N-H stretching vibrations in the range of 3100–3500 cm^{-1}, and the C-N stretching vibration band in the range of 1080–1360 cm^{-1}. (**d**) Spectrum of LMW chitosan NPs before and after being functionalizedwith Buforin II (blue) and pure Buforin II (black). Here, the absorbance bands analyzed contain the C=O stretching vibrations in the range of 1640–1690 cm^{-1}, the N-H bending vibrations in the range of 1550–1640 cm^{-1}, the N-H stretching vibrations in the range of 3100–3500 cm^{-1}, and the C-N stretching band in the range 1080–1360 cm^{-1}. (**e**) Spectrum of HMW chitosan NPs before and after functionalization with Buforin II (blue) and pure Buforin II (in black). Here, the absorbance bands analyzed contain the C=O stretching vibrations in the range of 1640–1690 cm^{-1}, the N-H bending vibrations in the range of 1550–1640 cm^{-1}, the N-H stretching vibrations in the range of 3100–3500 cm^{-1}, and the C-N stretching band in the range of 1080–1360 cm^{-1}.

3.3. Microscope Imaging (SEM, TEM and Confocal)

SEM images showed that gelatin nanoparticles, LMW, and HMW chitosan nanoparticles had a filamentous, round, and oval-like morphology, respectively (Figure 2).

TEM images of LMW chitosan NPs confirmed their morphology and showed that their nominal size of individual particles was 5 to 10 nm (Figure 3). These results demonstrated the NPs aggregate in solution, as evidenced by the increased size observed via DLS (see above). The confocal microscope showed HMW chitosan NPs–BUF-II–nanobioconjugates cellular internalization (Figure 4).

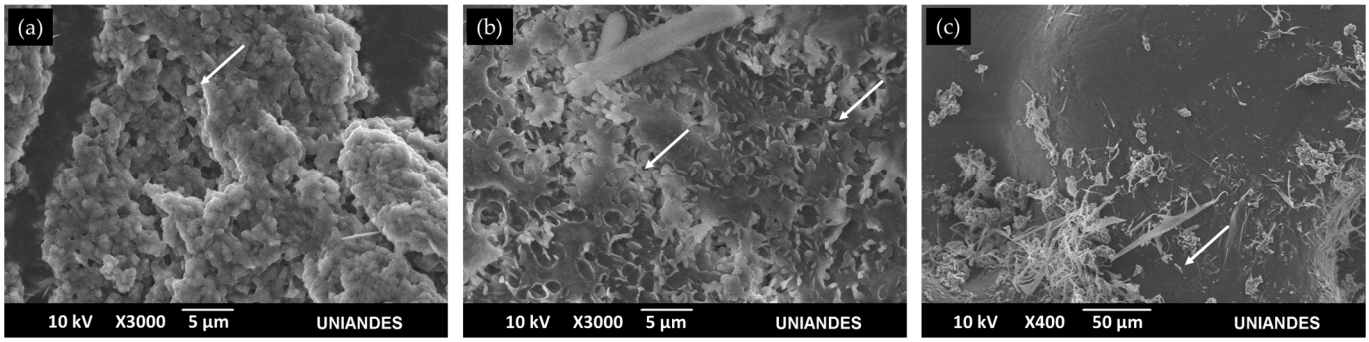

Figure 2. (**a**) SEM image of LMW chitosan NPs. (**b**) SEM image of HMW chitosan NPs. (**c**) SEM image of type B gelatin NPs. The white arrows point to the obtained materials.

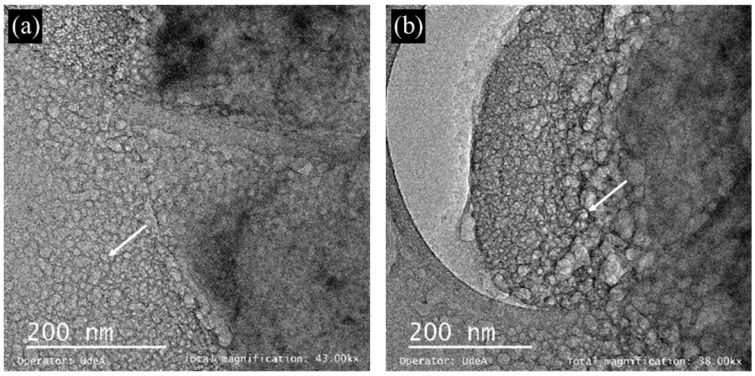

Figure 3. (**a**) TEM image of LMW chitosan NPs with a total magnification of 43kx. (**b**) TEM image of LMW chitosan NPs with a total magnification of 38kx.

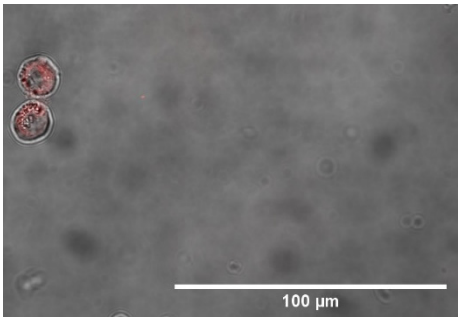

Figure 4. Confocal microscopy of THP-1 cells after being incubated with HMW chitosan NPs, which were previously functionalized with Buforin II and conjugated with rhodamine B.

4. Conclusions

The synthesis of the polymeric type B gelatin and chitosan NPs was successful, as was their functionalization with Buforin II and subsequent labeling with rhodamine B. Their low surface potential can explain their tendency to agglomerate. In addition, HMW chitosan NPs were successfully internalized in the human monocytic THP-1 cell line.

The different morphologies obtained for the NPs suggest the possibility for different internalization rates and intracellular trafficking routes, as indicated by recent studies that reported lower internalization rates for spherical NPs compared with oval NPs [27].

Accordingly, our future efforts explorewhether different potential intracellular routes can be enabled by NP type. This could be further exploited for targeting specific subcellular compartments.

Author Contributions: Conceptualization, J.C.C., C.M.-C. and L.H.R.; Methodology, data curation, and data analysis C.G. and J.C.C.; Formal analysis and investigation, C.G.; Validation, J.C.C., C.M.-C. and L.H.R.; Writing—original draft preparation, C.G.; Writing—review and editing, J.C.C., C.M.C. and L.H.R.; Supervision, J.C.C., C.M.-C. and L.H.R. All authors have read and agreed to the published version of the manuscript.

Funding: This work was funded by the Colombian Ministry of Science, Technology, and Innovation (Minciencias) Grants 689-2018, and ID 120380763212–PPTA # 8352.

Institutional Review Board Statement: Not applicable.

Informed Consent Statement: Not applicable.

Data Availability Statement: No new data were created or analyzed in this study. Data sharing is not applicable to this article.

Acknowledgments: The authors would like to thank the Department of Biomedical Engineering, Food and Chemical engineering and the Department of Electrical & Electronics Engineering at Universidad de los Andes for the financial and technical support.

Conflicts of Interest: The authors declare no conflict of interest.

References

1. Arms, L.; Smith, D.W.; Flynn, J.; Palmer, W.; Martin, A.; Woldu, A.; Hua, S. Advantages and limitations of current techniques for analyzing the biodistribution of nanoparticles. *Front. Pharmacol.* **2018**, *9*, 802.
2. Spicer, C.D.; Jumeaux, C.; Gupta, B.; Stevens, M.M. Peptide and protein nanoparticle conjugates: Versatile platforms for biomedical applications. *Chem. Soc. Rev.* **2018**, *47*, 3574–3620.
3. Behzadi, S.; Serpooshan, V.; Tao, W.; Hamaly, M.A.; Alkawareek, M.Y.; Dreaden, E.C.; Brown, D.; Alkilany, A.M.; Farokhzad, O.C.; Mahmoudi, M. Cellular uptake of nanoparticles: Journey inside the cell. *Chem. Soc. Rev.* **2017**, *46*, 4218–4244, doi:10.1039/c6cs00636a.
4. Bennet, D.; Kim, S. Polymer Nanoparticles for Smart Drug Delivery. In *Application of Nanotechnology in Drug Delivery*; InTech: London, UK, 2014.
5. Wang, W.; Gaus, K.; Tilley, R.D.; Gooding, J.J. The impact of nanoparticle shape on cellular internalisation and transport: What do the different analysis methods tell us? *Mater. Horizons* **2019**, *6*, 1538–1547, doi:10.1039/c9mh00664h.
6. Sharma, D.; Sharma, N.; Pathak, M.; Agrawala, P.K.; Basu, M.; Ojha, H. Nanotechnology-based drug delivery systems: Challenges and opportunities. In *Drug Targeting and Stimuli Sensitive Drug Delivery Systems*; Elsevier: Amsterdam, Netherlands, 2018; pp. 39–79, ISBN 9780128136898.
7. Selby, L.I.; Cortez-Jugo, C.M.; Such, G.K.; Johnston, A.P.R. Nanoescapology: progress toward understanding the endosomal escape of polymeric nanoparticles. *Wiley Interdiscip. Rev. Nanomedicine Nanobiotechnology* 2017, *9*.
8. Ramírez-Acosta, C.M.; Cifuentes, J.; Cruz, J.C.; Reyes, L.H. Patchy Core/Shell, Magnetite/Silver Nanoparticles via Green and Facile Synthesis: Routes to Assure Biocompatibility. *Nanomaterials* **2020**, *10*, 1857, doi:10.3390/nano10091857.
9. Cuellar, M.; Cifuentes, J.; Perez, J.; Suarez-Arnedo, A.; Serna, J.; Groot, H.; Muñoz-Camargo, C.; Cruz, J. Novel BUF2-magnetite nanobioconjugates with cell-penetrating abilities. *Int. J. Nanomedicine* **2018**, *Volume 13*, 8087–8094, doi:10.2147/IJN.S188074.
10. Perez, J.; Rueda, J.; Cuellar, M.; Suarez-Arnedo, A.; Cruz, J.C.; Muñoz-Camargo, C. Cell-Penetrating And Antibacterial BUF-II Nanobioconjugates: Enhanced Potency Via Immobilization On Polyetheramine-Modified Magnetite Nanoparticles. *Int. J. Nanomedicine* **2019**, *Volume 14*, 8483–8497, doi:10.2147/IJN.S224286.
11. Lopez-Barbosa, N.; Suárez-Arnedo, A.; Cifuentes, J.; Gonzalez Barrios, A.F.; Silvera Batista, C.A.; Osma, J.F.; Munõz-Camargo, C.; Cruz, J.C. Magnetite-OmpA Nanobioconjugates as Cell-Penetrating Vehicles with Endosomal Escape Abilities. *ACS Biomater. Sci. Eng.* **2020**, *6*, 415–424, doi:10.1021/acsbiomaterials.9b01214.
12. Lopez-Barbosa, N.; Garcia, J.G.; Cifuentes, J.; Castro, L.M.; Vargas, F.; Ostos, C.; Cardona-Gomez, G.P.; Hernandez, A.M.; Cruz, J.C. Multifunctional magnetite nanoparticles to enable delivery of siRNA for the potential treatment of Alzheimer's. *Drug Deliv.* **2020**, *27*, 864–875, doi:10.1080/10717544.2020.1775724.
13. Ramírez-Acosta, C.M.; Cifuentes, J.; Castellanos, M.C.; Moreno, R.J.; Muñoz-Camargo, C.; Cruz, J.C.; Reyes, L.H. PH-Responsive, Cell-Penetrating, Core/Shell Magnetite/Silver Nanoparticles for the Delivery of Plasmids: Preparation, Characterization, and Preliminary In Vitro Evaluation. *Pharmaceutics* **2020**, *12*, 561, doi:10.3390/pharmaceutics12060561.
14. Cervia, L.D.; Chang, C.C.; Wang, L.; Yuan, F. Distinct effects of endosomal escape and inhibition of endosomal trafficking on gene delivery via electrotransfection. *PLoS One* **2017**, *12*, doi:10.1371/journal.pone.0171699.

15. Dana, H.; Chalbatani, G.M.; Mahmoodzadeh, H.; Karimloo, R.; Rezaiean, O.; Moradzadeh, A.; Mehmandoost, N.; Moazzen, F.; Mazraeh, A.; Marmari, V.; et al. Molecular Mechanisms and Biological Functions of siRNA. *Int. J. Biomed. Sci.* **2017**, *13*, 48–57.
16. Smith, S.A.; Selby, L.I.; Johnston, A.P.R.; Such, G.K. The Endosomal Escape of Nanoparticles: Toward More Efficient Cellular Delivery. *Bioconjug. Chem.* **2019**, *30*, 263–272, doi:10.1021/acs.bioconjchem.8b00732.
17. Dizaj, S.M.; Jafari, S.; Khosroushahi, A.Y. A sight on the current nanoparticle-based gene delivery vectors. *Nanoscale Res. Lett.* **2014**, *9*, 1–9, doi:10.1186/1556-276X-9-252.
18. Azimi, B.; Nourpanah, P.; Rabiee, M.; Arbab, S. Producing gelatin nanoparticles as delivery system for bovine serum albumin. *Iran. Biomed. J.* **2013**, *18*, 34–40, doi:10.6091/ibj.1242.2013.
19. Carmona, E.R.; Plaza, T.; Recio-Sánchez, G.; Parodi, J. Generation of a protocol for the synthesis of chitosan nanoparticles loaded with florfenicol through the ionic gelation method. *Rev. Investig. Vet. del Perú* **2018**, *29*, 1195–1202, doi:10.15381/rivep.v29i4.15203.
20. Yan, S.C.; Li, Z.S.; Zou, Z.G. Photodegradation of rhodamine B and methyl orange over boron-doped g-C 3N4 under visible light irradiation. *Langmuir* **2010**, *26*, 3894–3901, doi:10.1021/la904023j.
21. ImageJ Available online: https://imagej.net/Welcome (accessed on Apr 19, 2021).
22. Rizvi, S.A.A.; Saleh, A.M. Applications of nanoparticle systems in drug delivery technology. *Saudi Pharm. J.* **2018**, *26*, 64–70, doi:10.1016/j.jsps.2017.10.012.
23. Foroozandeh, P.; Aziz, A.A. Insight into Cellular Uptake and Intracellular Trafficking of Nanoparticles. *Nanoscale Res. Lett.* **2018**, *13*, doi:10.1186/s11671-018-2728-6.
24. Kommareddy, S.; Shenoy, D.B.; Amiji, M.M. Gelatin Nanoparticles and Their Biofunctionalization. In *Nanotechnologies for the Life Sciences*; Wiley-VCH Verlag GmbH & Co. KGaA: Weinheim, Germany, 2007.
25. Ahsan, S.M.; Rao, C.M. The role of surface charge in the desolvation process of gelatin: Implications in nanoparticle synthesis and modulation of drug release. *Int. J. Nanomedicine* **2017**, *12*, 795–808, doi:10.2147/IJN.S124938.
26. Thakur, A.; Taranjit Preparation of chitosan nanoparticles: A study of influencing factors. In Proceedings of the AIP Conference Proceedings, Chandigarh, India, 23-26 February **2011**; Vol. 1393, pp. 299–300.
27. Nangia, S.; Sureshkumar, R. Effects of nanoparticle charge and shape anisotropy on translocation through cell membranes. *Langmuir* **2012**, *28*, 17666–17671, doi:10.1021/la303449d.